



Real-Gas Effects on the Aerodynamics of Blunt Cones as Measured in a Hypervelocity Range

C. J. Welsh, W. R. Lawrence, and R. M. Watt
ARO, Inc.

October 1979

Final Report for Period July 1975 — October 1978

Approved for public release; distribution unlimited

**ARNOLD ENGINEERING DEVELOPMENT CENTER
ARNOLD AIR FORCE STATION, TENNESSEE
AIR FORCE SYSTEMS COMMAND
UNITED STATES AIR FORCE**

NOTICES

When U. S. Government drawings, specifications, or other data are used for any purpose other than a definitely related Government procurement operation, the Government thereby incurs no responsibility nor any obligation whatsoever, and the fact that the Government may have formulated, furnished, or in any way supplied the said drawings, specifications, or other data, is not to be regarded by implication or otherwise, or in any manner licensing the holder or any other person or corporation, or conveying any rights or permission to manufacture, use, or sell any patented invention that may in any way be related thereto.

Qualified users may obtain copies of this report from the Defense Documentation Center.

References to named commercial products in this report are not to be considered in any sense as an indorsement of the product by the United States Air Force or the Government.

This report has been reviewed by the Information Office (OI) and is releasable to the National Technical Information Service (NTIS). At NTIS, it will be available to the general public, including foreign nations.

APPROVAL STATEMENT

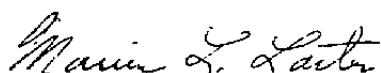
This report has been reviewed and approved.



MARSHALL K. KINGERY
Project Manager
Directorate of Technology

Approved for publication:

FOR THE COMMANDER



MARION L. LASTER
Director of Technology
Deputy for Operations

UNCLASSIFIED

REPORT DOCUMENTATION PAGE		READ INSTRUCTIONS BEFORE COMPLETING FORM
1 REPORT NUMBER AEDC-TR-79-33	2 GOVT ACCESSION NO.	3 RECIPIENT'S CATALOG NUMBER
4 TITLE (and Subtitle) REAL-GAS EFFECTS ON THE AERODYNAMICS OF BLUNT CONES AS MEASURED IN A HYPERVELOCITY RANGE		5 TYPE OF REPORT & PERIOD COVERED Final Report - July 1975 - October 1978
		6 PERFORMING ORG REPORT NUMBER
7 AUTHOR(s) C. J. Welsh, W. R. Lawrence, and R. M. Watt, ARO, Inc., a Sverdrup Corporation Company		8 CONTRACT OR GRANT NUMBER(s)
9 PERFORMING ORGANIZATION NAME AND ADDRESS Arnold Engineering Development Center/DOT Air Force Systems Command Arnold Air Force Station, Tennessee 37389		10 PROGRAM ELEMENT, PROJECT, TASK AREA & WORK UNIT NUMBERS Program Element 65807F
11 CONTROLLING OFFICE NAME AND ADDRESS Arnold Engineering Development Center/DOS Air Force Systems Command Arnold Air Force Station, Tennessee 37389		12. REPORT DATE October 1979
		13 NUMBER OF PAGES 26
14 MONITORING AGENCY NAME & ADDRESS (if different from Controlling Office)		15. SECURITY CLASS. (of this report) UNCLASSIFIED
		15a DECLASSIFICATION/DOWNGRADING SCHEDULE N/A
16 DISTRIBUTION STATEMENT (of this Report) Approved for public release; distribution unlimited.		
17 DISTRIBUTION STATEMENT (of the abstract entered in Block 20, if different from Report)		
18 SUPPLEMENTARY NOTES Available in DDC		
19 KEY WORDS (Continue on reverse side if necessary and identify by block number)		
blunt bodies nose cones aerodynamic characteristics hypervelocity	real-gas effects ballistics hypersonic characteristics	ranges (facilities) measurement pressure Reynolds number
20 ABSTRACT (Continue on reverse side if necessary and identify by block number)		
<p>A 1,000-ft hypervelocity range was used in a free-flight investigation of real-gas effects on the aerodynamics of blunted 10-deg semiangle cones. The tests were made using nitrogen and air test environments at a nominal velocity of 16,000 fps and at Reynolds number levels (based on model length and free-stream conditions) of about 0.4×10^6 and 2.0×10^6. Measurements indicate</p>		

UNCLASSIFIED

UNCLASSIFIED

20. ABSTRACT (Continued)

appreciable real-gas effects in the center-of-pressure and moment data. A discussion is also included of a new data reduction procedure devised to reduce nonlinear static stability data from small amplitude nonlinear motion histories.

PREFACE

The work reported herein was conducted by the Arnold Engineering Development Center (AEDC), Air Force Systems Command (AFSC). The Air Force project manager was Marshall K. Kingery. The results were obtained by ARO, Inc., AEDC Division (a Sverdrup Corporation Company), operating contractor for the AEDC, AFSC, Arnold Air Force Station, Tennessee. Some of the data presented in this report were obtained under sponsorship of the Army BMDATC, Huntsville, Alabama, for Science Applications, Inc., El Segundo, California, under ARO Project No. V41G-58. The work was done under ARO Project Nos. V32J-11, V32S-P4, and V41G-59A. The manuscript was submitted for publication on April 9, 1979.

The authors wish to acknowledge the contribution of E. O. Marchand formerly of ARO, Inc. for providing calculations of real-gas effects presented in this report. These calculations involved adapting the method-of-characteristics technique of Rakich (Ref. 12) to blunt cones for both real and perfect gases.

CONTENTS

	<u>Page</u>
1.0 INTRODUCTION	5
2.0 APPARATUS	5
3.0 TEST PROCEDURES	6
4.0 DATA REDUCTION	7
5.0 DATA UNCERTAINTY	14
6.0 RESULTS AND DISCUSSION	15
7.0 CONCLUDING REMARKS	23
REFERENCES	23

ILLUSTRATIONS

Figure.

1. Range G	6
2. Measured (α_c/α_m) Ratio for Different Levels of Cubic Nonlinearities	10
3. Effect of Motion Pattern Ellipticity on (α_c/α_m)	11
4. Capability of Reducing C_m Values from Motion Histories Using (α_c/α_m) = 0.87	12
5. Predicted Center-of-Pressure Location, $\alpha = 3$ deg (NASA-MOC)	16
6. Variation of c_p with Angle of Attack	17
7. Moment and Normal-Force Coefficients as Functions of Angle of Attack	19
8. Comparison of Damping Derivatives (Fig. 23 of Ref. 9)	21
9. Drag Coefficients for the Blunted Cones	22

TABLE

1. Test Conditions and Physical Measurements for the Cones	7
NOMENCLATURE	25

1.0 INTRODUCTION

The possibility of real-gas effects on the aerodynamics of high-speed vehicles has been a concern for several years. To investigate such effects, a series of shots utilizing blunt cones was made in the von Kármán Gas Dynamics Facility (VKF), AEDC, 1,000-ft Hyperballistic Range (G).

Both air and nitrogen range environments were used in the investigation, and, as it was assumed that nitrogen is a perfect gas for the present test conditions, real-gas effects were deduced from differences in the aerodynamic measurements made in these two test environments. Measurements were desired at small angles of attack for the blunt cones that can have appreciable force and moment nonlinearities even at the small angles. Satisfactory data reduction of the small amplitude, nonlinear flight histories required a reexamination of data reduction procedures used in free-flight testing.

The purpose of this report is to present the aerodynamic measurements obtained and to describe a data reduction procedure devised to reduce the nonlinear free-flight data.

2.0 APPARATUS

2.1 RANGE G

Range G consists of a 10-ft-diam, 1,000-ft-long tank that is contained within an underground enclosure (Fig. 1). It is a variable-density aerodynamic range and contains 53 dual-plane shadowgraph stations. Forty-three stations are positioned at nominal 20-ft intervals, yielding an 840-ft instrumented length. The other ten stations are located approximately 10 ft downrange of stations 5 through 10, 12, 13, 15, and 16. The angular orientation and position of most test configurations can be determined to within approximately ± 0.25 deg and ± 0.002 ft, respectively. A chronograph system measures intervals of flight time to within $\pm 2 \times 10^{-7}$ sec. The range vacuum pumping system provided the desired nominal range pressures of 20 and 50 torr in the present test program. The nominal operating temperature of the range is 76°F. The launcher used in the present test program is a two-stage, light-gas gun with a 2.5-in.-diam launch tube.

2.2 CONES AND SABOTS

The test configurations were 10-deg semiangle cones with nominal nose-to-base-radius-ratio (ψ) values of 0.07, 0.12, and 0.3. The cones tested had nominal base diameters of either 1.0 or 1.5 in. and were fabricated of aluminum except for the nosetips. All cones had

nosetips made of the tantalum-tungsten alloy Fansteel 60® to minimize possible in-flight nose geometry changes resulting from high aerodynamic heating conditions.

Sabots used were of a conventional four-component design and were fabricated of Lexan®. All cones were launched in an uncanted orientation relative to the sabot, and the initial angular disturbances to the cones were those arising from muzzle effects and from the cone-sabot separation process.

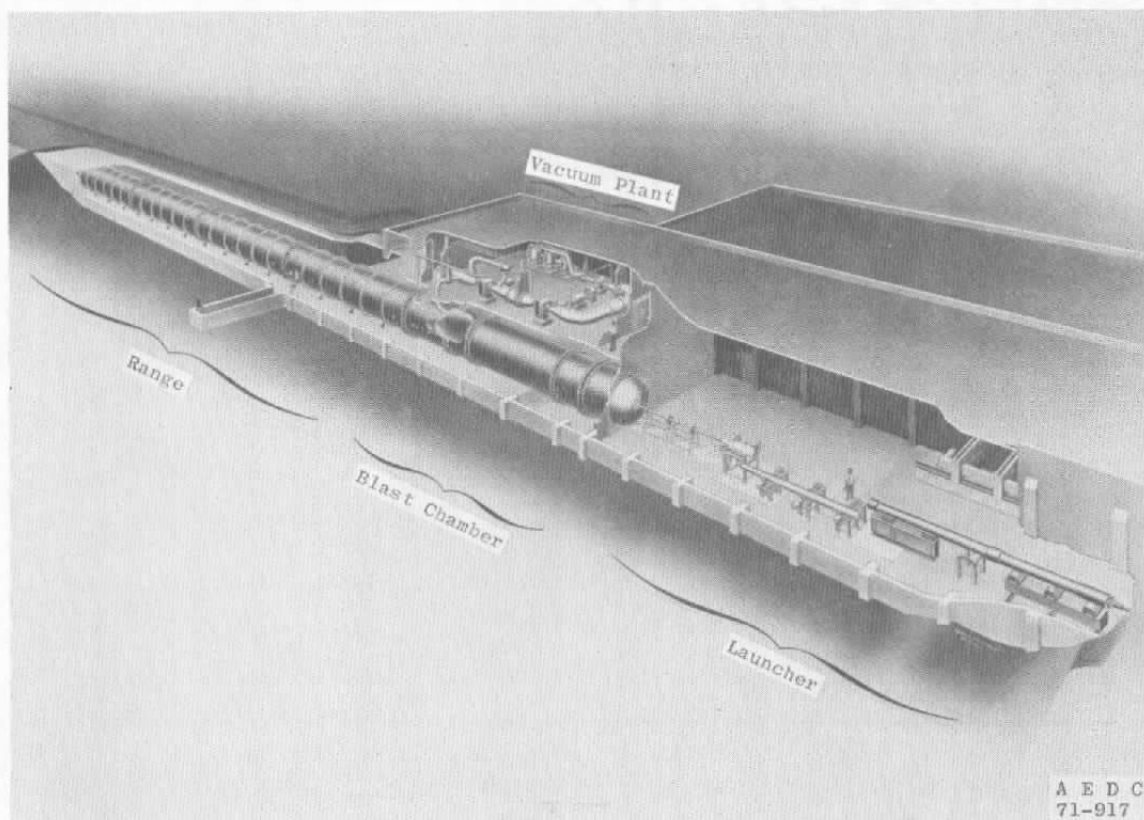


Figure 1. Range G.

3.0 TEST PROCEDURES

The initial step in the free-flight range testing procedure is to accelerate the model-sabot package to the desired velocity with use of a launcher. The sabot is then separated from the model in the blast tank portion of the range by aerodynamic forces. The model continues on its flight through the range, and its motion histories are monitored by the shadowgraph system. Model position-attitude-time measurements obtained from shadowgram and chronograph readings are used as inputs to the different data reduction computer programs used in the analysis of the motion histories. In this test program, air and nitrogen were used

as the two range environment fluids. Shot conditions and physical characteristics of the cones tested are tabulated in Table 1. The nominal velocity for the tests was 16,000 fps. Nominal Reynolds number levels were 0.4×10^6 and 2.0×10^6 .

Laser photography stations positioned along the range were used to monitor possible changes in the nose geometry of cones arising from aerodynamic heating during flight. Measurable nose geometry changes were observed only in the downrange portion of flights of the $\psi = 0.12$ cones in the air environment. The laser photographs permitted detecting changes in the effective nose diameter of a model to within about .005 in. Stability measurements presented for these cones were obtained using only the uprange portion of the motion histories (to shadowgraph station 17, the first 320 ft of the total 840-ft instrumented length of the range).

Table 1. Test Conditions and Physical Measurements for the Cones

Shot	Gas	m gm	d in.	$I_y \cdot 10^4$ in.-lb-sec ²	cg	ψ	V* fps	p _r torr	T _r deg F
1	Air	133.56	1.491	9.61	0.6200	0.1219	16,645	50.37	71.1
2	Nitrogen	130.96	1.489	9.38	0.6201	0.1209	15,650	49.14	71.6
3	Air	130.00	1.488	9.26	0.6201	0.1210	15,334	50.01	71.6
4	Air	130.83	1.488	9.48	0.6200	0.1210	16,554	50.25	72.3
5	Nitrogen	129.15	1.487	9.33	0.6210	0.1210	15,899	48.83	72.5
6	Nitrogen	130.70	1.487	9.40	0.6201	0.1210	15,809	48.53	72.2
7	Nitrogen	105.21	1.489	6.02	0.5784	0.3022	15,764	48.70	72.7
8	Air	117.15	1.488	6.12	0.5816	0.3091	16,001	49.84	72.2
9	Air	105.41	1.489	6.07	0.5741	0.3088	15,978	50.15	72.0
10	Nitrogen	20.66	0.9905	0.531	0.6303	0.0707	16,317	19.56	75.8
11	Nitrogen	20.67	0.9901	0.534	0.6304	0.0706	15,956	19.54	75.5
Ref. 8	Air	21.50	0.9928	0.539	0.6296	0.0690	15,187	20.01	74.0

NOTE: Roll rates of cone were < 0.6 deg/ft.

*Midrange Velocity

4.0 DATA REDUCTION

The numerical integration fitting technique (NIF technique) developed in recent years (e.g., Refs. 1 and 2) has been useful in reducing free-flight stability data for axisymmetric vehicles having nonlinear force and moment characteristics. Modifications in the motion equations discussed in Ref. 3 permitted an extension of the NIF technique to apply to vehicles with asymmetries. Such asymmetries include the primary aerodynamic asymmetries involving appreciable differences between C_{N_α} and C_{N_β} and between $|C_{m_\alpha}|$ and $|C_{m_\beta}|$.

A significant feature of the NIF technique is that motion histories of more than one flight can be fitted simultaneously. This multiple fit feature extends the capability of defining nonlinearities by permitting the use of different flights of the same configuration that had experienced large differences in mean amplitude levels. Experience has indicated that the amplitude change during a typical range model flight is usually not sufficient to reduce the nonlinear aerodynamic coefficients adequately from a single flight. This is particularly true for a shot having a small initial amplitude of about 5 deg or less.

In the present tests of blunt cones with nonlinear force and moment characteristics, initial cone amplitudes experienced in most of the shots were 4 deg or less; hence, a nonlinear data analysis using the NIF technique was therefore not feasible. In an attempt to provide a means to reduce the data adequately, quasi-linear data reduction procedures used in the past were reexamined, focusing on reducing center-of-pressure data.

For an ideal linear configuration, the moment coefficient can be written

$$C_m = C_{m_\alpha} \cdot \alpha \quad (1)$$

where C_{m_α} is a constant for different values of α . If the oscillatory motion histories of such a linear configuration are fitted with an NIF computer program (using only the linear terms of the program), C_{m_α} of Eq. (1) is one of the parameters defined. The amplitude of the motion interval fitted is of no concern as C_{m_α} is a constant and C_m can be defined for the α values of interest.

For a configuration having a nonlinear moment that can be described with a cubic nonlinearity (a cubic nonlinearity is normally assumed in the NIF technique), then

$$C_m = C_{m1\alpha} \cdot \alpha + C_{m3\alpha} \cdot \alpha^3 \quad (2)$$

If a motion history of such a configuration is fitted as above, using only the linear terms, then the motion-fitting program will define a quasi-linear moment parameter \overline{C}_{m_α} . The usefulness of \overline{C}_{m_α} values has been limited in the past because of lack of corresponding amplitude information available from the motion fit. For example, if measurements of \overline{C}_{m_α} were obtained from motion fits of a given configuration at different amplitude levels and they were approximately constant, then such measurements would have confirmed that the moment variation for the configuration was approximately linear. However, if different values were obtained for \overline{C}_{m_α} , then one would know only that the configuration had a nonlinear moment and that C_m , which is of primary concern in a nonlinear system, could not be defined directly.

Murphy (Ref. 4) and Rasmussen and Kirk (Ref. 5) presented two different analytical methods, each devised to determine nonlinear coefficients such as $C_{m1\alpha}$ and $C_{m3\alpha}$ of Eq. (2) individually, from a series of flight histories obtained for a model at different amplitude levels. If both $C_{m1\alpha}$ and $C_{m3\alpha}$ could be evaluated adequately, then the nonlinear variation of C_m with α could be determined. However, as is discussed later, neither method would be expected to be applicable for the small amplitude shots of the present investigation.

If a $\overline{C_{m\alpha}}$ value has been determined from a fit of an interval of motion history of a vehicle that in fact has a nonlinear moment coefficient defined by Eq. (2), then it follows that there is some effective amplitude, α_e , of the motion interval fitted that corresponds to the $\overline{C_{m\alpha}}$ such that C_m of Eq. (2) can be written

$$(C_m)_\alpha = \alpha_e = \overline{C_{m\alpha}} \cdot \alpha_e = C_{m1\alpha} \cdot \alpha_e + C_{m3\alpha} \cdot \alpha_e^3 \quad (3)$$

The obvious problem here is in relating α_e to the amplitude of the motion interval fitted. To accomplish this, the ratio (α_e/α_m) was used in this report. Here, α_m is the average of the midrange amplitude of the fitted interval and the mean of the initial and final amplitudes of the fitted interval. If α_e could be defined adequately, it would hold particular significance in that one point on the nonlinear C_m curve could be defined for each fitted $\overline{C_{m\alpha}}$ value without the problem of evaluating both $C_{m1\alpha}$ and $C_{m3\alpha}$ of Eq. (2).

The results of a brief study of the α_e concept for realistic free-flight test conditions indicate that the (α_e/α_m) ratio tends to be insensitive to the magnitude of the nonlinearity, to the type of motion pattern, and to the amplitude level involved for a fairly wide range of test conditions. These results are demonstrated in Figs. 2 through 4. To demonstrate the characteristics of α_e , a series of oscillatory motion histories (representative of Range G flights) was generated for different levels of cubic nonlinearities. These computer-generated "ideal" motion histories (excluding simulated experimental errors) were then fitted, using only linear terms of a motion-fitting program to obtain corresponding $\overline{C_{m\alpha}}$ values. The α_e values were then computed using the relationship obtained from Eq. (3)

$$\alpha_e = \sqrt{(\overline{C_{m\alpha}} - C_{m1\alpha})/C_{m3\alpha}} \quad (4)$$

$C_{m1\alpha}$ and $C_{m3\alpha}$ are both known parameters (used in generating the motion history), and $\overline{C_{m\alpha}}$ was obtained in the fitting of the ideal motion history. The results of those checks are shown in Fig. 2. The plotted moment curves represent a wide range of cubic nonlinearities and correspond to the generated motion histories used. A calculated moment curve for one of the blunt cones of the present investigation is also shown to indicate that the hypothetical moment curves used here are reasonable. All determined (α_e/α_m) values fell within a small band, and a value of 0.87 was selected as a representative value for the (α_e/α_m) ratio.

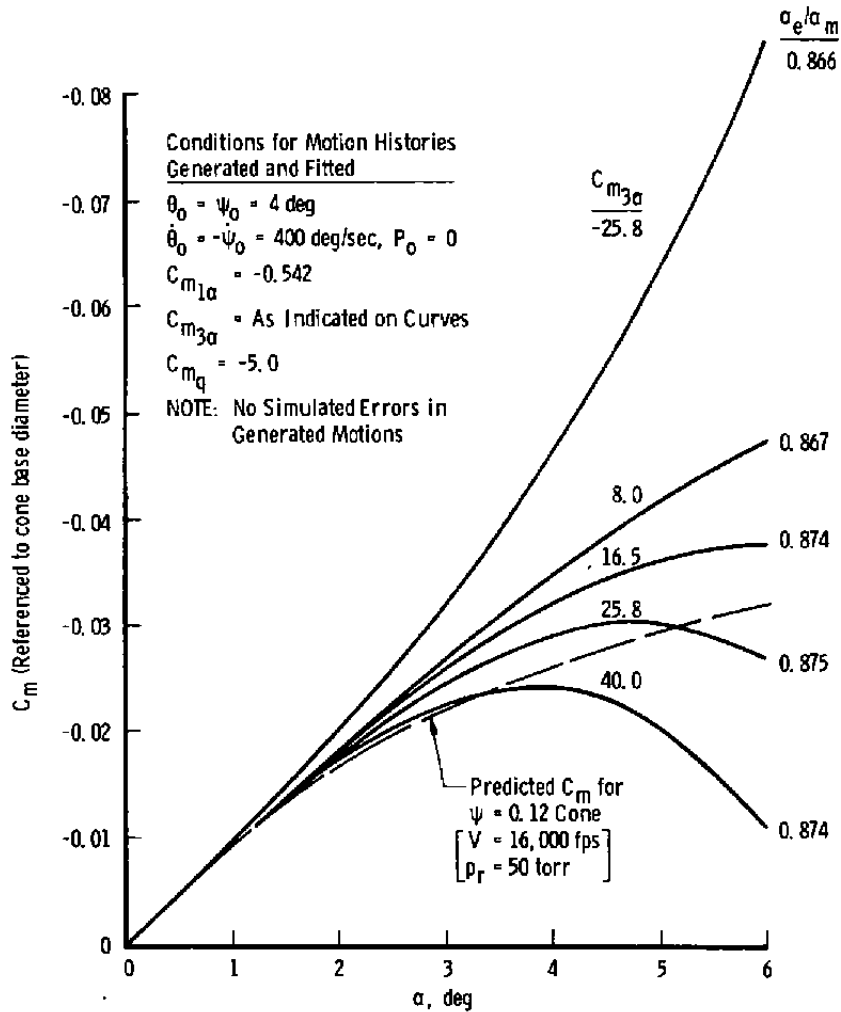


Figure 2. Measured (α_e/α_m) ratio for different levels of cubic nonlinearities.

The motion histories used in Fig. 2 (as noted in the figure) correspond to a fairly narrow elliptic pattern with an ellipticity (ratio of the lengths of the minor axis to the major axis) of 0.25. To show the effect of motion pattern shape on the (α_e/α_m) ratio, a series of additional motion histories was generated for one level of nonlinearity for a band of ellipticity values (representing planar to circular motion) and then fitted, again using only linear terms of the fitting program. Again, ideally generated motion histories were used. The results of those checks are shown in Fig. 3 in which (α_e/α_m) is plotted against ellipticity. The measurements indicate no detectable effect of ellipticity on the (α_e/α_m) ratio for ellipticity values up to about 0.5; however, (α_e/α_m) increases with further increases in ellipticity to a value of 1.0 for circular motion as would be expected. Ellipticity values for range flights are generally less than 0.3.

A demonstration of the effectiveness of the α_e concept in reducing nonlinear data is shown in Fig. 4. Motion histories were generated that corresponded to three different types

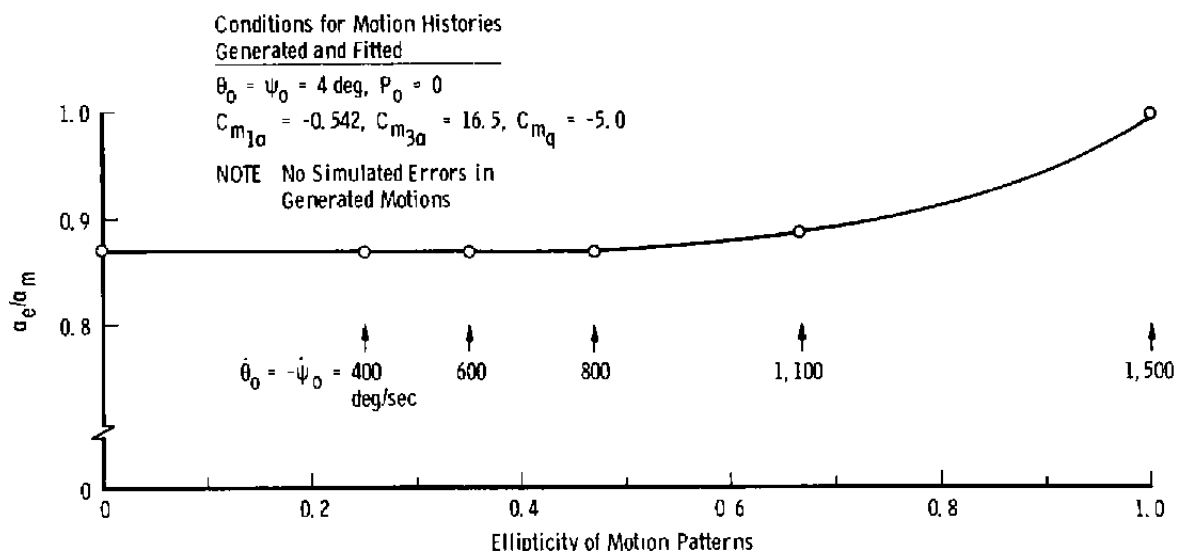


Figure 3. Effect of motion pattern ellipticity on $\{\alpha_e/\alpha_m\}$.

of nonlinearities (indicated in the figure); then simulated experimental errors (comparable to errors that would be experienced in Range G) were added to these motion histories. These generated histories with errors were then fitted (over different amplitude intervals), providing a \overline{C}_{m_α} value for each motion fit. The corresponding moment curves for the three types of nonlinearities used are shown in Fig. 4. Each plotted symbol is a C_m value obtained from an individual motion fit using the relation $C_m = \overline{C}_{m_\alpha} \cdot \alpha_e$ and 0.87 for (α_e/α_m) . The small deviations noted in the computed C_m values indicate that C_m can be determined quite well using the α_e concept for the three types of nonlinearities and different amplitude levels examined.

The results of the above investigation indicate that C_m values can be obtained quite well using the α_e concept from low-amplitude, nonlinear free-flight motion histories, given the following restrictions that (1) the test configuration is statically stable at zero angle of attack, (2) the magnitude of the nonlinear C_m curve at the maximum amplitude of the motion interval being fitted is not less than about 0.9 of the C_m peak value of the interval, (3) the ellipticity of the motion pattern is less than about 0.5, and (4) the model roll rate is small. The second restriction was dictated by excessive magnitude of deviations obtained in the fitted values of the quasi-linear force parameter (\overline{C}_{N_α}) and the damping parameter (\overline{C}_{m_q}) in motion fits of cases for which larger decreases in the moment curve existed. The magnitude of nonlinearity for a moment curve with an increasing slope is less restrictive in motion fits, and the ratio $(C_{m_{3\alpha}} \cdot \alpha_m^2 / C_{m_{1\alpha}})$ can be at least three times larger than the absolute value of this ratio for the moment curve with a decreasing slope.

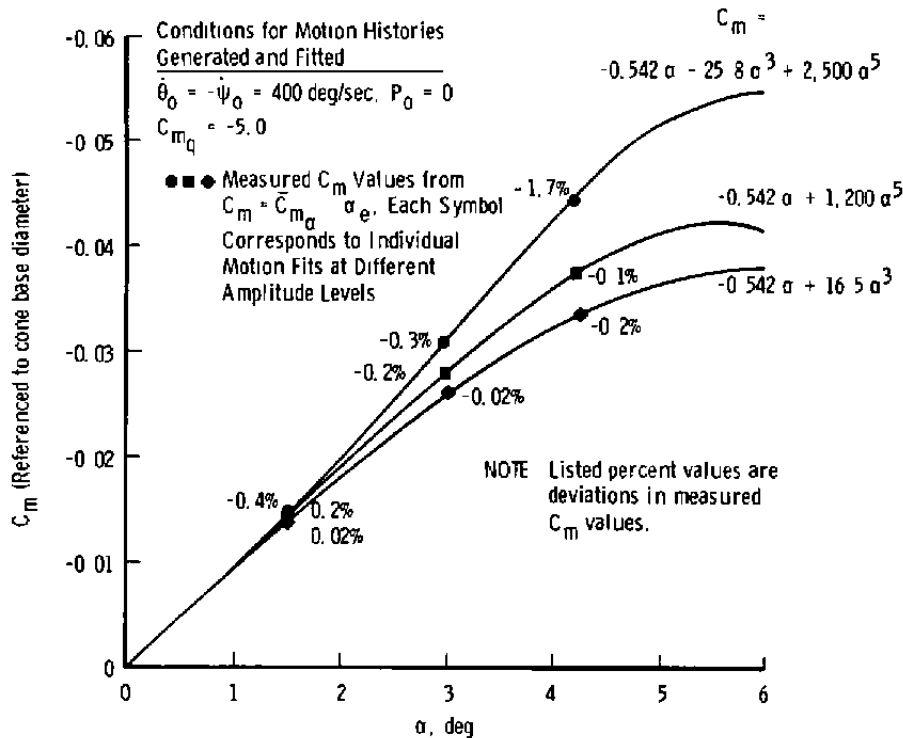


Figure 4. Capability of reducing C_m values from motion histories using $(\alpha_e/\alpha_m) = 0.87$.

Although the value of 0.87 for (α_e/α_m) was determined using cubic nonlinearities, measurements in Fig. 4 indicate that the insensitivity of this parameter permits its use with noncubic nonlinearities similar to those in Fig. 4. The insensitivity of the (α_e/α_m) ratio under the realistic free-flight test conditions of the present study is not too surprising. An exact solution was obtained by Kirk (Ref. 6) for a system having a corresponding cubic nonlinearity in the moment for the basic restraints of planar motion and zero damping. Although the method of Ref. 6 did not involve the use of the ratio (α_e/α_m) , this ratio can be calculated from presented information. Such calculations indicate that (α_e/α_m) is essentially a constant, within less than one percent (for planar motion and zero damping) for the above nonlinearity restrictions.

In using the α_e concept, the normal-force data is reduced similarly to the moment data. Hence, $C_N = \bar{C}_{N_\alpha} \cdot \alpha_e$, where \bar{C}_{N_α} is the quasi-linear normal-force parameter and is determined in the motion fitting process similarly to \bar{C}_{m_α} . Previous experience in reducing linear free-flight data indicates that C_{m_α} , a function of the frequency of the oscillatory motion, can be determined very well (within less than one percent) even when using only one cycle or so of the motion history. Only a portion of a typical Range G flight (which usually has three to four cycles) is required to define the motion frequency. Hence, the larger

deviations in the reduced C_m values of Fig. 4 indicate the limitation in defining α_e for those types of nonlinearities used. However, this is not the case with free-flight linear normal-force data. Here C_{N_α} is obtained from the fit of the oscillatory transverse motion history of the center of mass of the vehicle, and basic fitting limitations of this motion (transverse motion displacements are usually small) can result in errors up to ± 4 percent in C_{N_α} from a typical range flight. Hence, basic motion fitting errors can be expected to predominate over any α_e -related errors in determining C_N values from use of the quasi-linear normal-force parameter $\overline{C_{N_\alpha}}$.

Center-of-pressure locations can be determined quite well from free-flight measurements as indicated below.

The static margin (Δ) of a vehicle is defined

$$\Delta = (C_m/C_N) = (C_{m_\alpha}/C_{N_\alpha})_{\text{linear system}} \quad (5)$$

and the center-of-pressure location,

$$cp = cg + \Delta \quad (6)$$

For a combined error in the (C_m/C_N) ratio of 5 percent, a 3-percent static margin (referenced to body length), and a typical cg location of 63 percent of vehicle length, the resulting error in the center-of-pressure location would be less than 0.25 percent.

This method [using $(\alpha_e/\alpha_m) = 0.87$] should be adequate for handling a family of nonlinearities similar to those shown in Fig. 4 and is not restricted to just a cubic nonlinearity. It should be noted that the method is applicable in reducing free-flight data regardless of whether tests are made in aeroballistic ranges or in wind tunnels.

Although the ratio (α_e/α_m) is not used in either of the approximate methods of Refs. 4 and 5, sufficient information is presented for both methods to permit computing some values for (α_e/α_m) . Note that (α_e/α_m) values corresponding to each of these methods for a cubic nonlinearity and planar motion are in agreement with the results of the current study. However, available information was insufficient for such a comparison for nonplanar motion. It appears that the linear fitting programs that have been involved in the use of both of these methods (Refs. 4 and 5) incorporate the well-known epicyclic motion equation defined by Nicolaides in Ref. 7. In that type of a motion fitting program, the quasi-linear parameter, $\overline{C_{m_\alpha}}$, obtained in a fit of nonlinear nonplanar motion can be dependent on whether the model roll rate is measured and used as a known input to the program or on

whether the roll rate is permitted to float without restraint in the fitting process. It should be noted that in the present motion fitting investigation, all motion fits were obtained utilizing actual roll rates.

The drag coefficient, C_D , was obtained from the relation

$$C_D = -(2m/\rho S \bar{V}) (dV/dx) \quad (7)$$

where dV/dx is the mean slope of the curve of model velocity as a function of distance traveled, and \bar{V} is the mean model velocity during the interval of the flight trajectory being examined. The velocity data used are the average velocities between consecutive stations as obtained from the measured position-time history of the model. The term dV/dx is obtained by fitting a linear equation to the velocity-distance data by means of a least-squares procedure. Equation (1) is based on the assumption that C_D is constant during the flight interval of concern; Eq. (1) has been found to provide adequate results for the test conditions of the current program. Since the angle of attack of a model will normally vary along the trajectory, the drag coefficient obtained by this procedure corresponds to the mean total angle of attack experienced by the model. This mean angle of attack is defined by the relation

$$\bar{\delta^2} = [1/(L_2 - L_1)] \int_{L_1}^{L_2} \delta^2 dx \quad (8)$$

where $L_2 - L_1$ is the length of the flight interval over which C_D is computed.

The zero angle-of-attack drag coefficient is obtained from a linear extrapolation of a series of C_D measurements (obtained from different shots made at similar test conditions) as a function of δ^2 . With this drag reduction procedure, C_D can usually be reduced by using the complete flight history or by using only a portion of the flight. This procedure is useful for examining drag measurements in which possible nose-blunting effects, resulting from high aerodynamic heating conditions, may be involved.

5.0 DATA UNCERTAINTY

The estimated total uncertainties (2σ deviation) associated with measurements in this test program are as follows:

Parameter	Uncertainty, percent
C_D	1.5
C_m	1.0
C_N	4.0
cp	0.25
$C_{m_q} + C_{m_{\dot{\alpha}}}$	10.0

Any systematic errors in the above parameters have been estimated to be negligibly small.

6.0 RESULTS AND DISCUSSION

Predictions of real-gas effects have indicated that for some configurations the aerodynamic parameter particularly sensitive to such effects is the center of pressure. For example, predicted center-of-pressure locations (cp)* as a function of nose-to-base bluntness ratio (ψ) for a 10-deg semiangle cone are shown in Fig. 5. These predictions were obtained using a three-dimensional method-of-characteristics program referred to herein as NASA-MOC. For ψ values of about 0.12 (the primary ψ value of the present investigation) the predicted curves indicate that the cp in an air environment would be approximately one percent more forward than the cp in a nitrogen environment. However, a reversal occurs at higher ψ values, and for ψ about 0.3 the predicted curves indicate that cp in the air would be about one percent more aft than the cp in nitrogen. A shift in cp of this magnitude can be of much concern in the case of interceptor and maneuvering vehicles designed with small static margins.

All of the aerodynamic measurements obtained for 10-deg semiangle cones are presented in Figs. 6 through 9. Figure 6a shows both the cp measurements for the $\psi = 0.12$ cone and the corresponding calculated cp curves (NASA-MOC) for nitrogen and air environments. Each experimental point shown corresponds to a given range shot and is plotted at an angle of attack equal to α_c for that shot, consistent with the data reduction procedure discussed in Section 4.0. The cp measurements indicate significant real-gas effects; the level of the cp measurements in air is about 0.75 percent more forward than that measured in nitrogen. The calculated curves closely predict the shift in cp attributable to real-gas effects; however, they predict a cp about 0.5 percent more aft than the corresponding measured cp for both nitrogen and air. These observed differences in predicted and measured levels are not understood at present. It should be noted that all predictions in this report are for a sharp edge (zero radius) at the base of the cones, whereas the test cones were fabricated with a nominal edge radius of 0.03 in.

*Provided by E. O. Marchand, formerly of ARO, Inc.

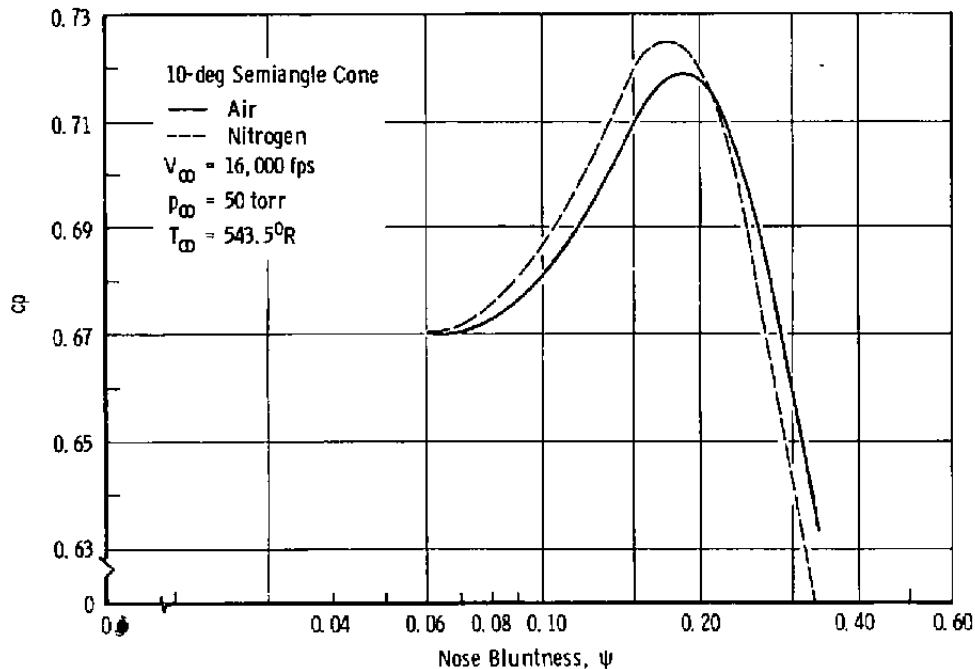
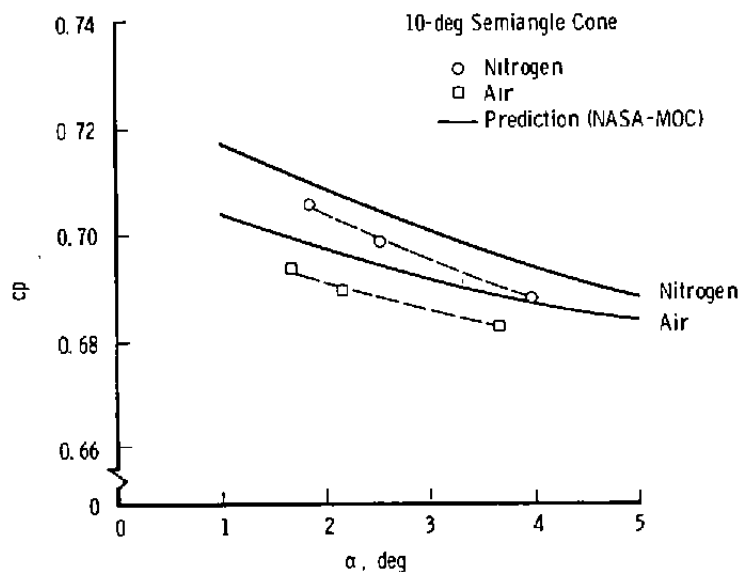
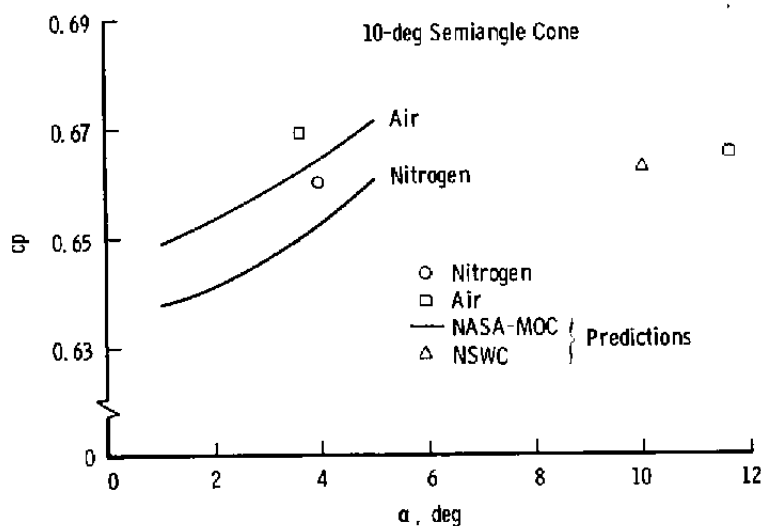


Figure 5. Predicted center-of-pressure location, $\alpha = 3$ deg (NASA-MOC).

Because of the significance of these cp measurements relative to both real-gas effects and differences from predicted values, the range measurements were scrutinized for possible sources of errors. For example, the sensitivity of the center-of-pressure location with nose bluntness as indicated in Fig. 5 would at first appear to be a factor of concern; however, the nose bluntness was measured for each model before launch (see Table 1), and these measurements indicated that the model noses had a bluntness ratio slightly greater than the design specification value of 0.12. Hence, any effects of bluntness deviations in model fabrication could only have caused decreases in the differences between measured and predicted cp values. Another possible source of error in the cp measurements is the nose-blunting effect caused by aerodynamic heating. As discussed previously, in-flight nose blunting was observed only in the air shots, and stability data were reduced using only the uprange portion of each of those three flights. Again, any undetected nose blunting in the uprange flights in air would have decreased the observed real-gas effects measured in the air and nitrogen shots. The results of such examinations indicate that any errors in the measured cp levels are appreciably smaller than the differences observed in Fig. 6a.

The cp measurements obtained and the corresponding predicted values are shown in Fig. 6b for the $\psi = 0.3$ cone. At the smaller amplitudes the cp measured in air is about one percent more aft than that measured in nitrogen. The calculated curves (NASA-MOC) predicted the real-gas effects well, but the predicted cp levels for both air and nitrogen were

a. $\psi = 0.12$ b. $\psi = 0.3$ Figure 6. Variation of c_p with angle of attack.

about one percent more forward than the measured values. The measured c_p in air at $\alpha \approx 11.5$ deg indicates that the predicted trend of aft movement of the c_p at the smaller amplitudes reverses above 5 deg. This is supported by the perfect-gas-calculated c_p point at $\alpha = 10$ deg in Ref. 8. Predictions from Ref. 8 (referred to as NSW) agree reasonably well with the NASA-MOC perfect-gas predictions up to 5 deg and, hence, are not shown herein. The NASA-MOC calculations were not available for $\alpha > 5$ deg.

There were two $\psi = 0.07$ cone shots (nitrogen environment) made primarily to assess possible real-gas effects in the dynamic stability data presented in Ref. 9; these measurements are discussed later in the report. Although these cones experienced large amplitude motion, cp measurements were obtained for them and are shown in Fig. 6c along with a cp data point for a $\psi = 0.07$ cone (Ref. 10). The calculated cp curve (air environment) shown in Fig. 6c agrees with the data from the low-amplitude shot discussed in Ref. 10; a small real-gas effect is indicated for the $\psi = 0.07$ cone by the air-nitrogen predictions. The cp values measured for the two high-amplitude shots indicate that the cp moves forward slightly with increasing angle of attack. The perfect-gas cp prediction (NSWC) at $\alpha = 10$ deg is in reasonable agreement with the high-amplitude experimental points.

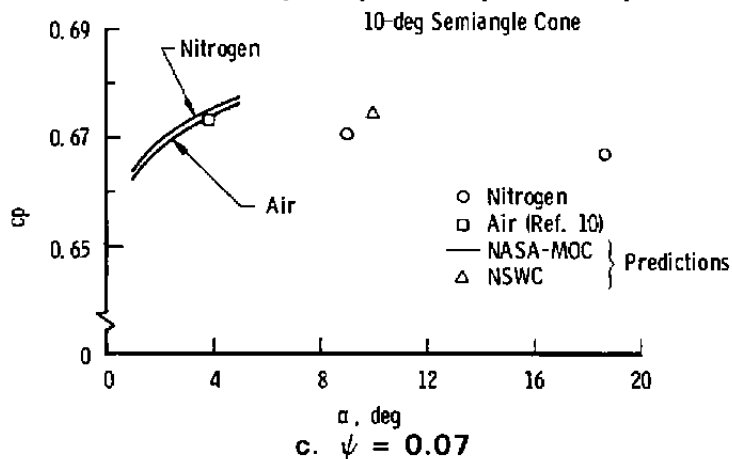


Figure 6. Concluded.

The C_m and C_N data for the $\psi = 0.07$, 0.12 , and 0.3 cones are shown in Fig. 7. Significant real-gas effects are apparent in the moment data for both the $\psi = 0.12$ and 0.3 cones at small angles. No appreciable real-gas effects were observed in the normal-force data obtained. The $\psi = 0.12$ moment data show appreciable nonlinear C_m variations measured for both air and nitrogen environments. The high-amplitude data points ($\alpha > 5$ deg) are in reasonable agreement with the small-amplitude data. The calculated curves predict the shifts in the force and moment data arising from real-gas effects well; however, some of the predicted C_m levels are noticeably displaced from the measured C_m levels. No normal-force data were obtained for the $\psi = 0.12$ cone shots because of the cones' experiencing small transverse motions, resulting primarily because the cones had larger static margins than are desirable for good normal-force measurements. The cp measurements for these shots were reduced using predicted C_N values at the corresponding α_c values. This is a sensible approach since normal-force predictions are generally quite good for cones. (The agreement of predicted and measured C_N values for the $\psi = 0.07$ and 0.3 cones at small amplitudes should be noted.)

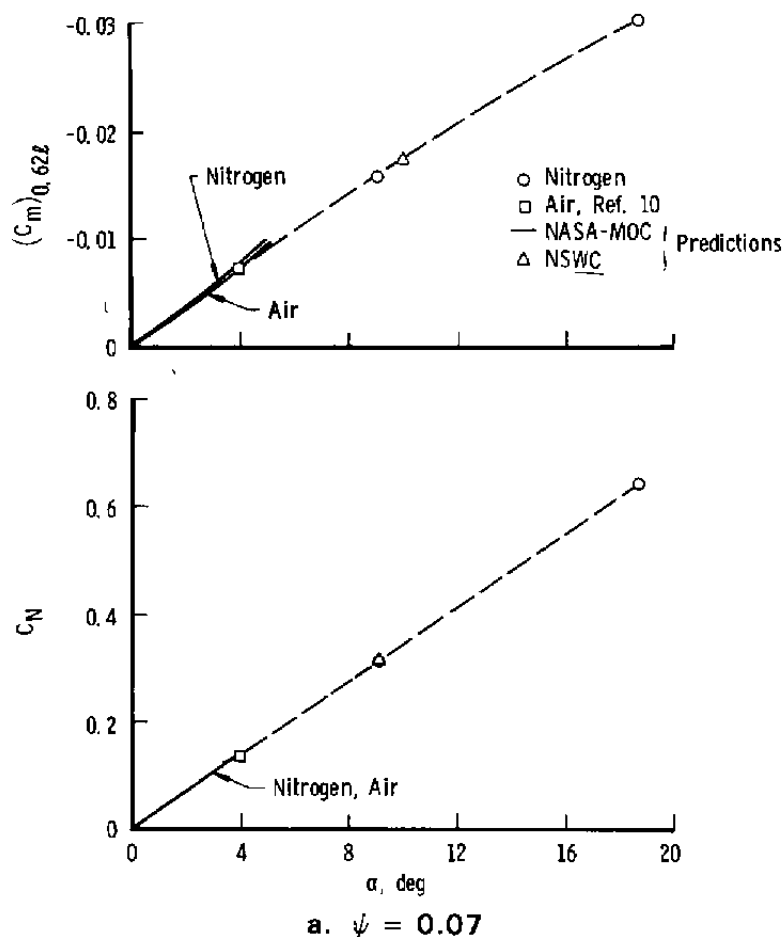
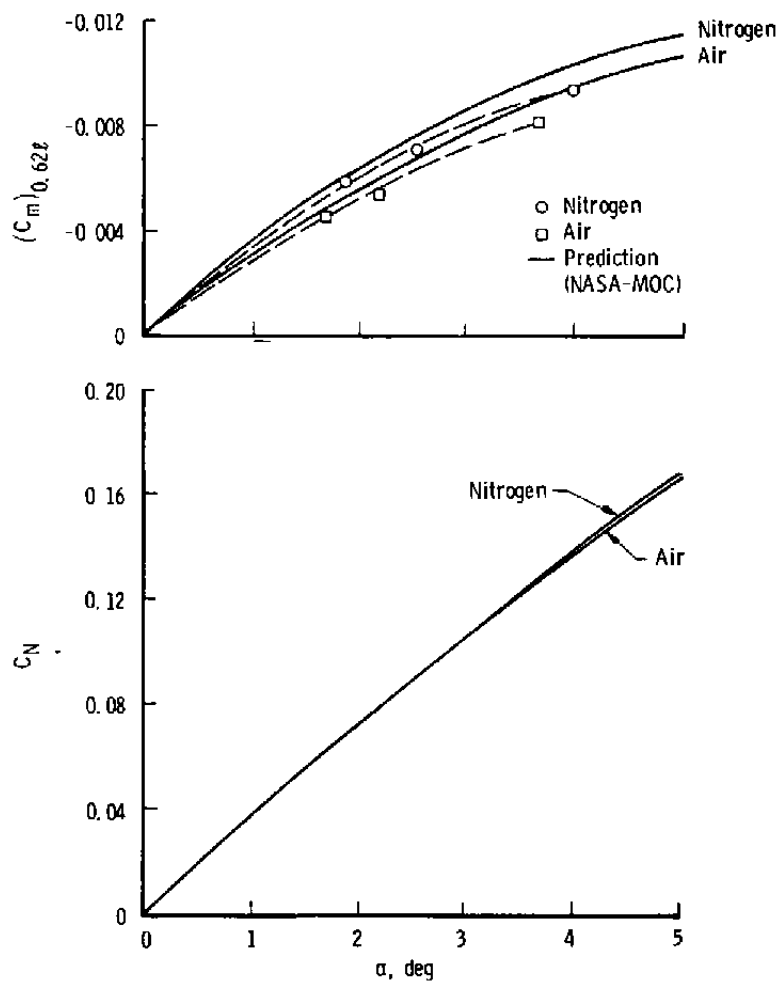
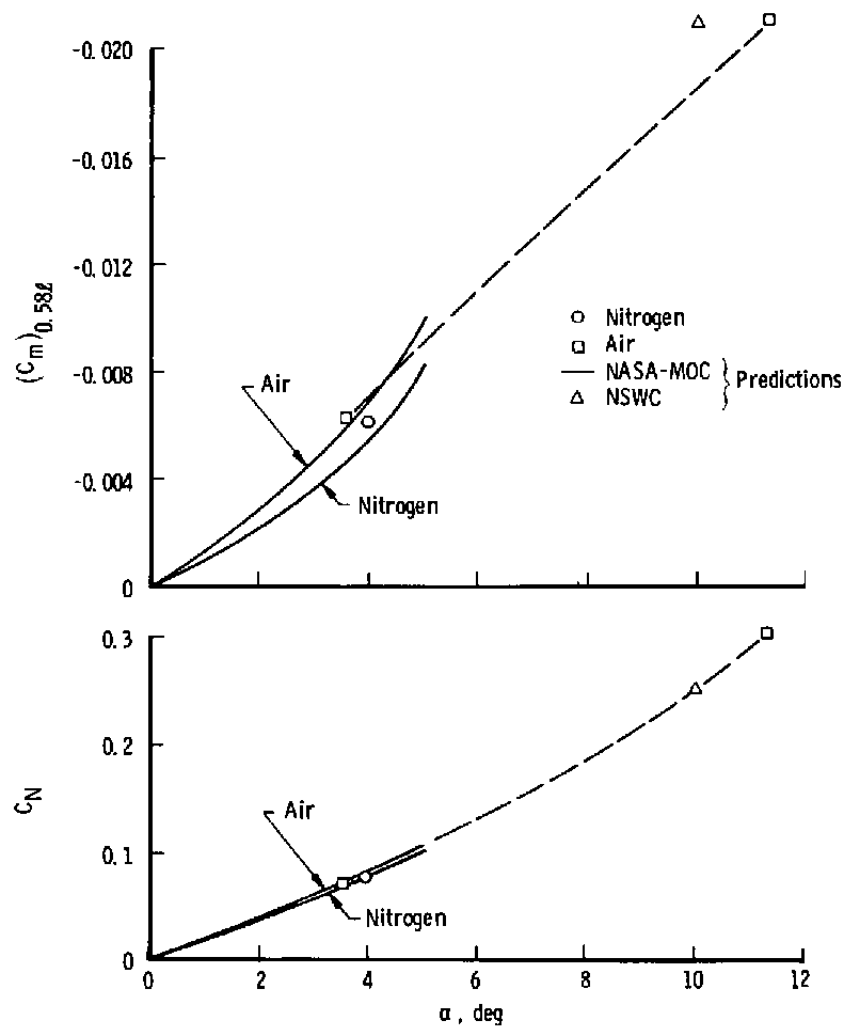


Figure 7. Moment and normal-force coefficients as functions of angle of attack.

Results of an aeroballistic range investigation made several years ago of the aerodynamic characteristics of 10-deg semiangle cones at high velocities were published in Ref. 9. Measurements of free-flight damping-in-pitch derivatives therein presented indicated an appreciable increase in damping with increasing Mach number between $M = 8$ and 16. The free-flight measurements were made in an air environment; there has been some concern that real-gas effects were reflected in those measurements. Figure 23 of Ref. 9 comparing the damping measurements has been replotted in Fig. 8. Also shown in Fig. 8 are two damping measurements obtained in the present investigation for the two $\psi = 0.07$ cones. Those shots, made in a nitrogen environment, agree with the previously obtained free-flight measurements made in air and, hence, indicate no significant real-gas effects in the damping measurements. After the two $\psi = 0.07$ cone shots were made in nitrogen, Ericsson and Reding (Ref. 11) showed that the increasing damping trend with Mach number between



b. $\psi = 0.12$
Figure 7. Continued.



c. $\psi = 0.3$
Figure 7. Concluded.

$M = 8$ and 16 is realistic when viscous crossflow effects are accounted for in the predicted damping values. It should be noted that the tests of Ref. 9 covered a wide range of amplitudes and indicated no detectable nonlinearities in the damping measurements for $\alpha \leq 0.07$.

Tunnel-Free Oscillation (Sting-Supported Models)

Sym	ψ	c_q	Re_L	$u d/2V$	Amplitude, deg	Facility
\diamond	0.016	60	$\approx 0.65 \times 10^6$	0.0026 to 0.007	$\alpha_0 = 0.5$ to 5.5	ARL
Δ	0	54.8	$\approx 0.56 \times 10^6$	0.0147	$\alpha_0 = 1.75$	LTV
\square	0	54.8	$\approx 0.165 \times 10^6$	0.0115	$\alpha_0 = 1.75$	LTV
Γ	0.017	58.7	0.35×10^6	0.0024 to 0.0125	$\alpha_{mean} = 1.5$	VKF
\diamond	0.0167	55	0.25×10^6	0.023	$\alpha_{mean} = 2$	VKF
∇	0.017	58.7	0.28×10^6	0.0019 to 0.0107	$\alpha_0 = 1.5$	ARL

NOTE:

Additional points added to figure are all for comparable test conditions of range data of Ref. 9.

$\diamond \psi = 0.07$ (Air) from Ref. 9

$\nabla \psi = 0.07$ (Nitrogen) from Present Test

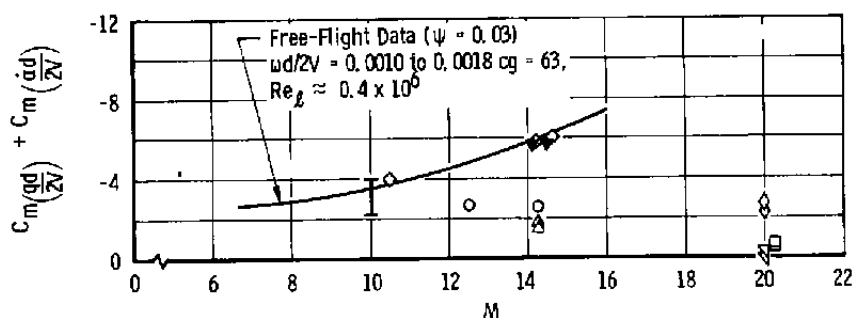
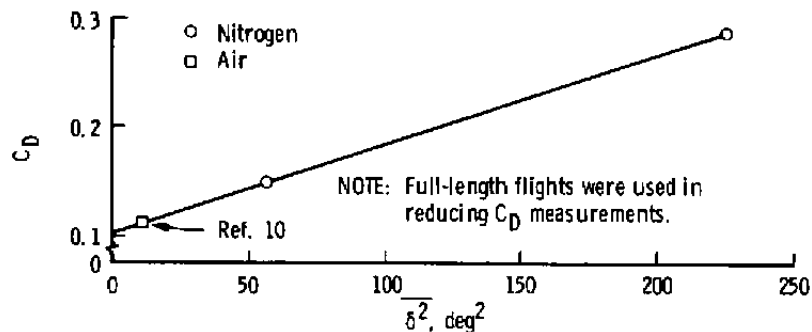


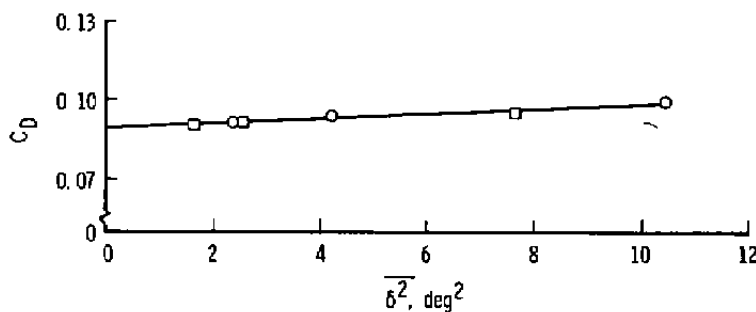
Figure 8. Comparison of damping derivatives (Fig. 23 of Ref. 9).

Drag measurements for the three blunt-cone configurations are shown in Fig. 9. No detectable real-gas effects on the drag coefficient were observed. Of additional interest are the shots for the $\psi = 0.12$ cone made in an air environment. As noted previously, these shots experienced nose blunting (caused by aerodynamic heating) during their flights. The effect of nose geometry changes resulting from aerodynamic heating and corresponding ablation effects on C_D apparently tends to be compensating (see Fig. 9b, drag measurements reduced over total length of flights) for the present test conditions. Such compensating effects on C_D have been observed in other test programs.

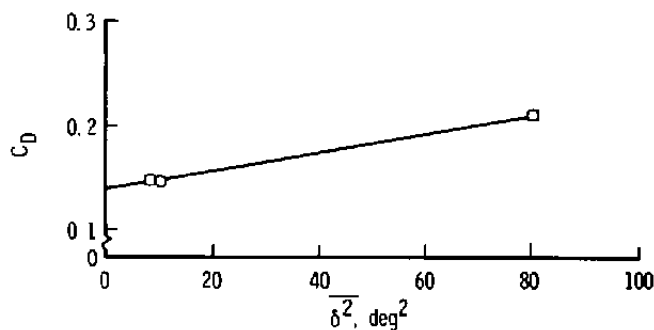
In summary, the test measurements indicate significant real-gas effects in the current center-of-pressure and moment data. Consistency in these measurements indicates that the devised procedure for reducing small-amplitude, nonlinear, static stability data is quite feasible. Because of the large inertia values involved in the present tests of the $\psi = 0.12$ and 0.3 cones, obtaining damping derivatives for these cones was infeasible.



a. $\psi = 0.07$



b. $\psi = 0.12$



c. $\psi = 0.3$

Figure 9. Drag coefficients for the blunted cones.

7.0 CONCLUDING REMARKS

A free-flight investigation of real-gas effects on the aerodynamics of blunted 10-deg semiangle cones was made. The nominal test velocity was 16,000 fps, and the nominal Re_ℓ levels were 0.4×10^6 and 2.0×10^6 . The test models were $\psi = 0.07$, 0.12 , and 0.3 cones.

Real-gas effects as evaluated from measurements using different test environments (air and nitrogen) were appreciable in the center-of-pressure and moment data. For example, shifts in the cp position of up to one percent of the cone length were measured. No significant real-gas effects were observed in the normal-force or drag data. A comparison using damping data previously published indicated no apparent real-gas effects on the damping derivatives for the $\psi = 0.07$ cone. Measured changes in the center-of-pressure and moment data arising from real-gas effects were predicted well with the NASA-MOC method.

The aerodynamic measurements made in the present test program indicate that the new procedure devised to reduce nonlinear static stability data from small-amplitude motion histories is feasible. The data reduction procedure is applicable for free-flight tests made in either aeroballistic ranges or wind tunnels.

REFERENCES

1. Chapman, Gary T. and Kirk, Donn B. "A Method for Extracting Aerodynamic Coefficients from Free-Flight Data." *AIAA Journal*, Vol. 8, No. 4, April 1970, pp. 753-758.
2. Whyte, Robert H. and Hathaway, Wayne H. "Aeroballistic Range Data Reduction Technique Utilizing Numerical Integration." AFATL-TR-74-41, February 1974.
3. Welsh, C. J. and Lawrence, W. R. "Motion Analysis Procedure for Asymmetric Vehicles." AEDC-TR-75-158 (AD-A024674), May 1976.
4. Murphy, C. H. "Free Flight Motion of Symmetric Missiles." BRL Report No. 1216, July 1963.
5. Rasmussen, Maurice L. and Kirk, Donn B. "On the Pitching and Yawing Motion of a Spinning Symmetric Missile Governed by an Arbitrary Nonlinear Restoring Moment." NASA TN D-2135, March 1964.

6. Kirk, Donn B. "A Method for Obtaining the Nonlinear Aerodynamic Stability Characteristics of Bodies of Revolution from Free-Flight Tests." NASA TN D-780, March 1961.
7. Nicolaides, John D. *On the Free-Flight Motion of Missiles Having Slight Configurational Asymmetries*. BRL Report 858 (AD26405), June 1953.
8. Morrison, A. M., Solomon, J. M., Ciment, M. and Ferguson, R. E. "Handbook of Inviscid Sphere-Cone Flow Fields and Pressure Distribution." Vol. II, NSWC/WOL/TR-75-45, December 1975.
9. Welsh, C. J., Winchenbach, G. L., and Madagan, A. N. "Free-Flight Investigation of the Aerodynamic Characteristics of a Cone at High Mach Numbers." *AIAA Journal*, Vol. 8, No. 2, February 1970, pp. 294-300.
10. Welsh, C. J. and Winchenbach, C. L. "Free-Flight Investigation of Ablation Effects on the Stability of Conical Reentry Configurations." AEDC-TR-71-242 (AD736455), February 1972.
11. Ericsson, Lars E. and Reding, J. Peter. "Viscous Interaction or Support Interference — The Dynamicist's Dilemma." *AIAA Journal*, Vol. 16, No. 4, April 1978, pp. 363-368.
12. Rakich, John V. "A Method of Characteristics for Steady Three Dimensional Supersonic Flow with Application to Inclined Bodies of Revolution." NASA-D-5341, October 1969.

NOMENCLATURE

C_D	Mean drag coefficient for flight
C_m	Moment coefficient
C_N	Normal force coefficient
$C_{m(qd/2V)} + C_{m(\alpha d/2V)}$	Damping in pitch derivatives
$C_{m\alpha}, C_{n\beta}$	Moment derivatives
$\overline{C}_{m\alpha}$	Quasi-linear moment derivative
$C_{m1\alpha}, C_{m3\alpha}$	Nonlinear moment coefficients
$C_{N\alpha}, C_{N\beta}$	Normal force derivatives
$\overline{C}_{N\alpha}$	Quasi-linear normal force derivative
cg	Center of gravity, measured from nose of the cone and referenced to the cone length
cp	Center-of-pressure location measured from the nose of the cone and referenced to the cone length
d	Cone base diameter
I_y	Moment of inertia (relative to a transverse axis)
l	Cone length
m	Cone mass
P_o	Initial roll rate
p_r	Range pressure
Re_l	Reynolds number based on free-stream conditions and cone length

T_r	Range temperature
V	Cone velocity
α	Total angle of attack (small angles) or sine of total angle-of-attack
α_e	Effective angle of attack, see Eq. (3)
α_m	Mean amplitude of motion interval being fitted
δ	Total angle of attack
$\overline{\delta^2}$	Mean total angle of attack, see Eq. (8)
θ_o, ψ_o	Euler angles (initial values)
$\dot{\theta}_o, \dot{\psi}_o$	Time derivatives of the Euler angles (initial values)
ψ	Cone nose bluntness ratio (nose radius/base radius)
ω	Model frequency

SUBSCRIPT

$x.xx\ell$	Moment reference point location
∞	Ambient conditions

NOTE: All coefficients and derivatives are referenced to the cone base area. The reference length for all moment coefficients and moment derivatives is the cone length, except where indicated otherwise.